Article

Quantum Dot Based Luminescent Nanoprobes for Sigma-2 Receptor Imaging

Maria Laura Pati, Elisabetta Fanizza, Sonja Hager, Diana Groza, Petra Heffeter, Amelita Grazia Laurenza, Valentino Laquintana, Maria Lucia Curri, Nicoletta Depalo, Carmen Abate, and Nunzio Denora

Mol. Pharmaceutics, **Just Accepted Manuscript** • DOI: 10.1021/acs.molpharmaceut.7b00825 • Publication Date (Web): 11 Dec 2017

Quantum Dot Based Luminescent Nanoprobes for Sigma-2 Receptor Imaging

Maria Laura Pati,[†,a] Elisabetta Fanizza,[‡,§,a] Sonja Hager,[#] Diana Groza,[#] Petra Heffeter,[#] Amelita Grazia Laurenza,[‡] Valentino Laquintana,[†] Maria Lucia Curri,[§] Nicoletta Depalo,[§,] Carmen Abate[†,]* and Nunzio Denora[†]*

[†] Dipartimento di Farmacia-Scienze del Farmaco, Università degli Studi di Bari Aldo Moro, Via Orabona 4, I-70125 Bari, Italy.

[§]Istituto per i Processi Chimico-Fisici - IPCF - SS Bari, Consiglio Nazionale delle Ricerche, c/o Dipartimento di Chimica, Università degli Studi di Bari Aldo Moro Via Orabona 4, 70125 Bari, Italy

[‡]Dipartimento di Chimica, Università degli Studi di Bari Aldo Moro, Via Orabona 4, I-70125 Bari, Italy

[#]Department of Medicine I, Institute of Cancer Research and Comprehensive Cancer Center of the Medical University, Medical University of Vienna, Borschkegasse 8a, A-1090 Wien, Austria

[*]Corresponding Author: n.depalo@ba.ipcf.cnr.it Istituto per i Processi Chimico-Fisici - IPCF - SS Bari, Consiglio Nazionale delle Ricerche, c/o Dipartimento di Chimica, Università degli Studi di Bari Aldo Moro Via Orabona 4, 70125 Bari, Italy
carmen.abate@uniba.it Dipartimento di Farmacia-Scienze del Farmaco, Università degli Studi di Bari Aldo Moro, Via Orabona 4, I-70125 Bari, Italy

Abstract. The increasing importance of sigma-2 receptor as target for the diagnosis and therapy of tumours paves the way for the development of innovative optically traceable fluorescent probes as tumour cell contrast and therapeutic agents. Here, a novel hybrid organic-inorganic nanostructure is developed by combining the superior fluorescent properties of inorganic quantum dots (QDs), coated with a hydrophilic silica shell (QD@SiO_2 NPs), the versatility of the silica shell and the high selectivity for sigma-2 receptors of the two synthetic ligands, namely the 6-[(6-aminohexyl)oxy]-2-(3-(6,7-dimethoxy-3,4-dihydroisoquinolin-2(1*H*)-yl)propyl)-3,4-dihydroisoquinolin-1(2*H*)-one (MLP66) and 6-[1-[3-(4-

cyclohexylpiperazin-1-yl)propyl]-1,2,3,4-tetrahydronaphthalen-5-yloxy]hexylamine (TA6). Therefore, the proposed nanostructures represent a challenging alternative to all previously studied organic small fluorescent molecules, based on the same sigma-2 receptor affinity moieties. Flow cytometry and confocal fluorescence microscopy experiments, respectively, on fixed and living cancerous MCF7 cells, which overexpress the sigma-2 receptors, prove the ability of functionalized (QD@SiO_2-TA6 and QD@SiO_2-MLP66) NPs to be internalized and demonstrate their affinity to the sigma-2 receptors, ultimately validating the targeting properties conveyed to the NPs by sigma-2 ligand conjugation. The presented QD-based nanoprobes possess a great potential as *in vitro* selective sigma-2 receptor imaging agent and, consequently, could provide a significant impact to future theranostic applications.

Keywords: hybrid nanostructure, fluorescent bioimaging, quantum dots, sigma-2 receptor

1. Introduction. In spite of the overall decrease of mortality rate in the past 20 years,[1] cancer is still the second leading cause of death, as some tumours are still characterized by an increasing incidence (e.g. liver, pancreas, thyroid, leukemia tumour), and expected to overtake the prevalence of cardiovascular diseases within the next years. One of the major open challenges in treating cancers is to increase the tumour specificity of chemotherapeutic agents in order to reduce the often severe side effects causing damage to normal tissues and organs.[2] This goal can be accomplished by developing an efficient targeting delivery nanosystem, able to direct selective binding to cancer cells. Indeed, clinical nanotechnology based strategies have proven that nanoparticle based delivery platforms can effectively enhance therapeutic efficacy, improve targeted delivery to tumours and active cellular uptake while simultaneously reducing side effects.[3-6] In this scenario, several inorganic colloidal nanoparticles (NPs), and nanocrystals (NCs), including plasmonic gold NPs,[7-8] luminescent quantum dots (QDs),[9-10] superparamagnetic iron oxide NPs[11-12] as well as

nanoheterostructures[13] have demonstrated a vast potential as targeted therapeutic and/or diagnostic nanovectors.[14-16] Indeed, their high surface to volume ratio, their peculiar size dependent physicochemical properties, such as optical or magnetic characteristics, and their ability to be surface engineered with a large variety of ligands to enhance their affinity towards target sites point out the enormous capability of such colloidal nanostructures.[17-22] Among the synthetic ligands that can be conjugated to NP surface for an active targeting of tumour tissues, small molecules offer a number of advantages, such as high degree of purity, scalability of production, lack of immunogenicity as well as elevated affinity and selectivity for the receptors.[23] Receptors overexpressed in tumour cells represent promising targets for binding cancer cells. In this perspective, two subtypes of sigma receptors (namely subtype-1, sigma-1 receptor and subtype-2, sigma-2 receptor), overexpressed in cancer cells from animal and human origins, are gaining increasing attention as tumour targets. While the subtype-1 of sigma receptors has been already cloned and crystallized,[24] the subtype-2 has still to be clearly identified. In fact, sigma-2 has been first proposed as a histone protein,[25] and later as the progesterone receptor membrane component 1 (PGRMC1) protein complex,[26] with strong evidence supporting the non-identity of the sigma-2 protein with the PGRMC1.[27-29] Only recently, this receptor has been proposed as the endoplasmic reticulum (ER)-resident membrane protein TMEM97.[30] Despite the still unclear identification, the interest in the sigma-2 receptor research is recently increasing as an exceptional candidate tumour imaging target, since it is expressed about 10-fold more in proliferating tumour cells than in quiescent tumour cells. In addition, ligand binding to this receptor can result in tumour cell death *via* both apoptotic and non-apoptotic mechanisms.[31] Therefore, sigma-2 proteins represent promising targets for the therapy and diagnosis of tumours, with significant preliminary results obtained from cell culture and from preclinical models of aggressive tumours such as the pancreas carcinoma.[32-34] In addition, clinical phase I studies for the diagnosis of different tumours are already ongoing.[35-36] In literature, few reports on the use of sigma-2 receptors

ligands conjugated to inorganic NPs for their targeted delivery into cancer cells have been presented.[37-39] A new class of conjugates composed of gold nanocages and a ligand specific to sigma-2 receptors (SV119) have been proposed[37] as a multifunctional and theranostic platform for cancer targeting. Furthermore, anisamide ligand-conjugated gold nanospheres have been investigated for the targeting of sigma receptors, although the preferential binding of anisamide to either subtypes has not been demonstrated.[40-41] On this basis and in order to support sigma-2 receptors for selective cancer targeting, in this work, novel sigma-2-directioning luminescent nanostructures have been prepared by conjugating luminescent semiconductor QDs, with two different specific sigma-2 receptor ligands. Luminescent QDs have been selected as fluorescent contrast agents due to their superior optical properties with respect to conventional organic fluorophores, including stability to photobleaching, long fluorescence (PL) lifetime, enabling long-term and sensitive imaging and wide absorption spectrum.[17,18,42-43] In particular, amine-functionalized luminescent silica-coated (CdSe)ZnS QDs, namely (QD@SiO_2-NH_2 NPs) have been successfully conjugated to two structurally different small molecules, the 6-[(6-aminohexyl)oxy]-2-(3-(6,7-dimethoxy-3,4-dihydroisoquinolin-2(1*H*)-yl)propyl)-3,4-dihydroisoquinolin-1(2*H*)-one (MLP66) and 6-[1-[3-(4-cyclohexylpiperazin-1-yl)propyl]-1,2,3,4-tetrahydronaphthalen-5-yloxy]hexylamine (TA6).[44] The ligand structures have been purposely designed on the bases of two of the highest affinity and selectivity sigma-2 receptor ligands previously reported (the 2-(3-(6,7-dimethoxy-3,4-dihydroisoquinolin-2(1*H*)-yl)propyl)-6-methoxy-3,4-dihydroisoquinolin-1(2*H*)-one (1)[45] for the MLP66 and 1-cyclohexyl-4-[3-(5-methoxy-1,2,3,4-tetrahydronaphthalen-1-yl)-n-propyl]piperazine (PB28)[46] for the TA6, respectively). This synthetic strategy has allowed to fabricate two different types of single nano-objects, each combining the high affinity of the specific ligand towards sigma-2-receptors and the peculiar emission properties of the QD@SiO_2 NPs. The obtained highly luminescent nanoplatforms are the first examples of sigma-2-targeted QD-based nanostructures that have been obtained

and represent powerful optically traceable tools to investigate sigma-2 receptors at the subcellular level. Original insights on the sigma-2 receptor physiological role and its mechanism of action could thus be obtained in future by taking advantage of the superior fluorescent properties of QD@SiO_2 while tracing the path to the targeted delivery of death-inducing payloads to sigma-2-overexpressing cancer cells. In this perspective, the diagnostic potential of the proposed luminescent targeted nanostructures could be extended to cancer therapy, or to adjuvant anticancer treatment.

2. Materials and Methods.

2.1 Chemistry. Column chromatography was performed with 60 Å pore size silica gel as the stationary phase (1:30 w/w, 63-200 μm particle size from ICN). Melting points were determined in open capillaries on a Gallenkamp electrothermal apparatus. ^{1}H NMR (300 MHz) spectra were recorded on a Mercury Varian spectrometer. $CDCl_3$ was used as solvent to record ^{1}H NMR unless otherwise stated. The following data were reported: chemical shift (d) in ppm, multiplicity (s = singlet, d = doublet, t = triplet, m = multiplet), integration and coupling constant(s) in Hertz. Recording of mass spectra was done on an Agilent 6890-5973 MSD gas chromatograph/mass spectrometer and on an Agilent 1100 series LC-MSD trap system VL mass spectrometer; only significant m/z peaks, with their percentage of relative intensity in parentheses, are reported. Chemicals were from Aldrich, Alfa Aesar or TCI and were used without any further purification. Details of the synthesis for the sigma-2 receptor ligands are reported in the Supplementary Information file.

*2.1.1 6-(2,5-Dimethylpyrrol-1-yl)hexan-1-ol (**2**)*. To a solution of 6-amino-1-hexanol (0.8 g, 8 mmol) in anhydrous toluene (20 mL), acetonyl acetone (0.93 g, 8.9 mmol) and a catalytic amount of *p*-toluensulfonic acid were added and the mixture was refluxed for 6 h during which water was removed through a Dean Stark apparatus. The

solvent was then removed under reduced pressure and the red dense oil obtained was purified by column chromatography (CH_2Cl_2/AcOEt, 8:2) to provide the title compound as an orange oil (82% yield); GC/MS *m/z*: 301 (M^+, 195), 108 (100).

*2.1.2. 6-(2,5-Dimethylpyrrol-1-yl)hexyl methansulfonate (**3**).* To a solution of compound **2** (17.77 mmol, 2.88 g) in dry CH_2Cl_2 (30 mL) cooled in a dry ice bath, Et_3N (37 mmol, 5.14 mL) and methansulfonyl chloride (17.72 mmol, 1.36 mL) were added dropwise and the solution was stirred at the same temperature for 1 h. Water was then added to the reaction (15 mL) and the mixture was extracted with CH_2Cl_2 (3 × 20 mL), the organic phases collected and dried (Na_2SO_4). The crude obtained was purified by column chromatography (AcOEt/$_n$-Hexane; 1:1) affording the title compound as a brown oil (70% yield); ^{1}H NMR (300 MHz) δ 1.35-1.85 [m, 8H, $(CH_2)4$], 2.20 [s, 6H, $(ArCH_3)_2$], 3.00 (s, 3H, SO_2CH_3), 3.72 (t, 2H, J = 7.7 Hz, CH_2N), 4.22 (t, 2H, J = 6.5 Hz, CH_2N), 5.70 (s, 2H, aromatic); LC-MS (ESI^+) *m/z*: 296 $[M+Na]^+$; LC-MS-MS 296: 178, 108.

*2.1.3. 6-Hydroxy-3,4-dihydro-isoquinolin-(2H)-1-one (**4**).* CCl_3COOH (4.0 g) and 5-hydroxyindan-1-one (2.70 mmol, 4.0 g) were heated up to 90 °C until the mixture melt. NaN_3 (0.35, 5.4 mmol) was added and the mixture was warmed at 90 °C for 4 h. The reaction vessel was then cooled, added with ice and neutralized with $KHCO_3$ (saturated solution). The aqueous phase was extracted with AcOEt (3 × 10 mL) and the organic phases were collected and dried (Na_2SO_4) to provide a crude solid that was purified by column chromatography (CH_2Cl_2/AcOEt, 1:1), to provide the title compound as a white solid (42% yield)); ^{1}H NMR (CD_3OD) δ 2.88 (t, 2H, J = 6.6 Hz $ArCH_2$), 3.45 (t, 2H, J = 6.7 Hz $NHCH_2$), 6.60-6.70 (m, 2H, aromatic), 7.75-7.85 (m, 1H, aromatic); LC-MS (ESI^+) *m/z*: 296 $[M+Na]^+$; LC-MS-MS 296: 178, 108.

*2.1.4. 6-Benzyloxy-2-(3-chloropropyl)-3,4-dihydro-isoquinolin-(2H)-1-one (**6**).* To a suspension of NaH (4.35 mmol, 0.104 g) in anhydrous DMF (5 mL) cooled on an ice

bath, 6-benzyloxy-3,4-dihydro-isoquinolin-(2*H*)-1-one **5** (1.74 mmol, 0.44 g) dissolved in the same solvent (10 mL) was added dropwise. The mixture was stirred at the same temperature for 15 min and afterwards added with 1-Bromo-3-chloropropane (1.91 mmol, 0.27 mL), and left under stirring at room temperature for 1h. Excess of NaH was then quenched with water upon cooling, and the solvent was evaporated under reduced pressure. The crude residue was taken up with water and extracted with CH_2Cl_2 (3 × 20 mL), the organic phases were collected and dried (Na_2SO_4) to provide a crude mixture that was purified by column chromatography (CH_2Cl_2/AcOEt, 8:2), to provide the title compound as a white solid (78% yield); GC/MS *m/z*: 329 (M^+, 195), 294 (30), 91 (100).

2.1.5. 2-(3-(6,7-Dimethoxy-3,4-dihydroisoquinolin-2(1H)-yl)propyl)-3,4-dihydroisoquinolin-6- benzyloxy-1(2H)-one (7). To a solution of **6** (1.35 mmol, 0.45 g) in DMF (20 mL), 6,7-dimethoxy-1,2,3,4-tetrahydroisoquinoline (1.49 mmol, 0.29 g) and K_2CO_3 (1.50 mmol, 0.21 g) were added and the mixture was warmed under stirring at 100 °C for 6 h and at room temperature overnight. After cooling to room temperature, the solvent was evaporated under vacuum and the residue was treated with H_2O and extracted with CH_2Cl_2 (3 × 15 mL). The collected organic layers, were dried (Na_2SO_4) and concentrated under reduced pressure to provide a crude residue which was purified by column chromatography with CH_2Cl_2/MeOH (95:5) as eluent, to provide the title compound as a dense yellow oil (40% yield); LC-MS (ESI^+) *m/z*: 509 $[M+Na]^+$; LC-MS-MS 509: 403.

*2.1.6. 2-(3-(6,7-Dimethoxy-3,4-dihydroisoquinolin-2(1H)-yl)propyl)-3,4-dihydroisoquinolin-6- hydroxy-1(2H)-one (**8**).* A solution of **7** (0.49 mmol, 0.24 g) in MeOH (7 mL) was added with Pd 10% on activated charcoal and stirred under H_2 (4 atm) overnight. The mixture was filtrated through Celite to remove the catalyst and the filtrate was evaporated under vacuum to provide a brown oil residue which was

purified by column chromatography with CH_2Cl_2/MeOH (9:1) as eluent, to provide the title compound as a waxy solid (55% yield); ^{1}H NMR δ 1.85-2.00 (m, 2H, $CH_2CH_2CH_2$), 2.49 (t, 2H, J = 6.6 Hz, NCH_2), 2.65-2.75 (m, 2H, NCH_2), 2.85-2.95 (m, 4H, $ArCH_2$), 3.29 (t, 2H, J = 6.6 Hz, $CONCH_2$), 3.56-3.60 (m, 3H, $CONCH_2$ and OH, D_2O exchanged), 3.67 (s, 2H, NCH_2Ar), 3.85 (s, 6H, OCH_3), 6.32 (d, 1H, J = 2.4 Hz, aromatic), 6.51 (s, 1H, aromatic), 6.56 (s, 1H, aromatic), 6.71 (dd, 1H, J = 8.5 Hz, J' = 2.4 Hz, aromatic), 7.88 (d, 1H, J = 8.5 Hz, aromatic).

*2.1.7. 2-[3-(6,7-Dimethoxy-3,4-dihydroisoquinolin-2(1H)-yl)propyl]-6-{[6-(2,5-dimethyl-1H-pyrrol-1-yl)hexyl]oxy}-3,4-dihydroisoquinolin-1(2H)-one (**9**)*. To a solution of the intermediate compound **8** (0.16 mmol, 0.066 g) in CH_3CN (10 mL), mesyl derivative **3** (0.2 mmol, 0.055 g) and K_2CO_3 (0.4 mmol, 0.055 g) were added and the mixture was refluxed under stirring overnight. The solvent was evaporated under vacuum and the residue was treated with H_2O and extracted with AcOEt (3 × 10 mL). The collected organic layers were dried (Na_2SO_4) and concentrated under reduced pressure to provide a dense yellow oil, which was purified by column chromatography with CH_2Cl_2/MeOH (98:2) as eluent. The title compound was obtained as a yellow oil (65% yield); LC-MS (ESI^+) *m/z*: 596 $[M+Na]^+$.

2.1.8. 6-[(6-Aminohexyl)oxy]-2-(3-(6,7-dimethoxy-3,4-dihydroisoquinolin-2(1H)-yl)propyl)-3,4-dihydroisoquinolin-1(2H)-one (**MLP66**). $NH_2OH{\cdot}HCl$ (0.57 mmol, 0.04 g) was added to a solution of the intermediate **9** (0.11 mmol, 0.07 g) in EtOH/H_2O (5 mL, 1/1) and the mixture was refluxed under stirring for 24 h. After cooling, NaOH (1.15 mmol, 0.046 g) was added to the mixture, which was refluxed under stirring for further 24 h. The solution was then concentrated under reduced pressure and the residue was taken up with H_2O (3 mL) and extracted with AcOEt (3 × 5 mL). The collected organic layers were dried (Na_2SO_4) and concentrated under reduced pressure to provide a dense yellow oil, which was purified as oxalate salt and recrystallized

from MeOH/Et_2O (60% yield); ^1H NMR δ 1.35-1.90 (m, 10H, $CH_2(CH_2)_4$ and $CH_2CH_2CH_2$), 1.95-2.00 (m, 2H, NCH_2), 2.58-2.98 (m, 8H, 2 NCH_2, 2 $ArCH_2$), 3.55-3.65 (m, 6H, $CONCH_2$ and $ArCH_2N$), 3.83 (s, 3H, OCH_3), 3.85 (s, 3H, OCH_3), 3.95-4.02 (m, 2H, OCH_2), 6.55 (s, 1H, aromatic), 6.60 (s, 1H, aromatic), 6.65-6.83 (m, 2H, aromatic), 7.92-8.05 (m, 1H, aromatic); LC-MS (ESI^+) *m/z*: 518 $[M+Na]^+$; 496 $[M+H]^+$; LC-MS-MS 496: 303, 204, 176.

2.2 Synthesis and characterization of silica-coated QDs

2.2.1 Materials. Cadmium oxide (99.5% powder, CdO), Trioctylphosphine oxide (99%, TOPO), t-Butylphosphonic acid (98%, tBuPOH), Hexadecylamine (technical grade 90%, HDA, Fluka), Tributylphosphine (97%, TBP), Selenium (99.99% powder, Se), Sulfur (99.9999% powder, S), Trioctylphosphine (90%, TOP), Diethylzinc solution (1 M in heptanes, Et_2Zn), Hexamethyldisilathiane (HMST) orthosilicate (98% d = 0.934 g/mL, TEOS), aqueous ammonia solution (d = 0.900 g/mL, NH_4OH), 5-polyoxyethylene nonylphenylether (Igepal CO-520, Mn=441), 3-Aminopropyl)triethoxysilane (97%, APS), Ninhydrin, 2,6-lutidine (98%) bis(sulfosuccinimidyl)suberate (≥95%, BS3), boric acid and dimethyl sulfoxide (DMSO) were all purchased from Sigma Aldrich.

2.2.2 Synthesis of QD@SiO_2 NPs functionalized with sigma-2 receptor ligands. CdSe@ZnS QDs with emission centered at 597 nm (d = 4 nm and relative standard deviation $\sigma_{\%}$ = 20%, for absorption and emission spectra and transmission electron micrograph, see Supporting Information Figure S1), synthesized as previously reported, [47,48] was coated with a silica shell by means of water-in-oil microemulsion approach (6 mL of ciclohexane, 50 µL of CdSe@ZnS QD solution at $1.8 \cdot 10^{-4}$ M, 350 µL IGEPAL-CO520, 200 µL ammonia solution 28%, 50 µL TEOS). The QD@SiO_2 NPs were dispersed in 2 mL of ethanol. Amine groups were grafted on NP surface by

condensation reaction carried out at high pH condition between siloxane groups of the APS and silanol groups at the silica surface, (0.7 mmol of APS added to 400 μL of QD@SiO_2 NPs diluted to 2 mL ethanol), and the degree of functionalization was measured by a ninhidrine assay, able to titrate the amine groups at the surface (1 mg/mL of QD@SiO_2-NH_2 with [NH_2] of nearly $4 \cdot 10^{-3}$M).[13, 47] TA6 was crosslinked at the QD@SiO_2-NH_2 NPs by using BS^3 as cross coupling agent in 2 mL of DMSO/borate buffer 50 mM at pH 8.5 (nearly 2:1). In particular, 500 μL of QD@SiO_2-NH_2 NPs in ethanol ($2 \cdot 10^{-6}$mol of NH_2 groups) were centrifuged, redispersed in 500 μL of DMSO/borate buffer (1:1) and mixed with an equimolar solution of TA6 in 1 mL of DMSO/borate buffer (4:1). Finally, an excess of BS^3, $2 \cdot 10^{-5}$ mol in 500 μL of DMSO/borate buffer (1:1) was added and the reaction mixture stirred for 2 h before being quenched by addiction of 10 μL of TRIS HCl. QD@SiO_2-TA6 NPs were finally collected by repeated cycles of centrifugation at 7000×g and redispersion in DMSO and finally suspended in DMSO for the spectroscopic characterization and in H_2O for hydrodynamic diameter, size distribution colloidal stability and *in vitro* experiments. Functionalization of QD@SiO_2-NH_2 NPs with MLP66 was carried out by using the same crosslinking reactions protocol.

The TA6 and MLP66 content in QD@SiO_2–TA6 and QD@SiO_2–MLP66 NPs respectively was determined by spectrofluorometric characterization prior to construction of a calibration curve. In particular, fluorescent spectra of each ligand (λ_{ex}= 300 nm) at different concentration were recorded. The calibration curve was obtained by plotting the integrated area of the emission band in the wavelength range between 330 and 500 nm and 330-580 nm, for TA6 and MLP66, respectively, versus ligand concentration.

2.3 Transmission Electron Microscopy (TEM). TEM images were acquired by using a JEOL 100, operating at 100 kV and a Quemesa Olympus CCD 11 Mp Camera.

Starting from a NP suspension in ethanol, the samples were deposed on 300 mesh amorphous carbon-coated Cu grid by dipping and evaporation of the solvent. Size statistical analysis (average NP size and relative standard deviation (σ%) for each NP sample) was performed by means of a freeware Image J analysis program, to provide information on the NP size distribution.

2.4 Spectroscopic characterization. For the spectroscopy characterization, performed at room temperature the following equipments were used: UV-Vis absorbance spectra were recorded by a Cary Varian 5000 UV-visible-NIR, spectrophotometerfluorescent spectra were recorded by spectrofluorimeter Fluorolog 3 (HORIBA Jobin-Yvon) equipped with double chromator reticles in excitation and emission and absolute PL QY were measured dispersing the NP samples in DMSO and using the spectrofluorimeter equipped with an integration sphere. Infrared spectra in Fourier transform infrared (FTIR) mode with a spectral resolution of 4 cm^{-1} were recorded with a Perkin-Elmer Spectrum One FTIR spectrometer equipped with a DTGS (deuterated triglycine sulphate) detector.

2.5 Particle size, size distribution and surface charge. Hydrodynamic diameter (size) and size distribution (reported in terms of numbers and polydispersity index (PDI), respectively) for the colloidal nanosystem samples were determined at each functionalization step by means of dynamic light scattering (DLS). The investigation was perfomed by diluting the NP aqueous solution (borate buffer, 50 mM, pH 8.5) in demineralized water. Similarly, NP aqueous solutions (borate buffer, 50 mM, pH 8.5) were diluted in KCl aqueous solution (1 mM) for ζ-potential measurements, carried out by using a laser doppler velocimetry (LDV) performed in triplicates. All these analysis were carried out using a Zetasizer Nano ZS, Malvern Instruments Ltd., Worcestershire, UK (DTS 5.00).

2.6 Cell biology.

2.6.1 Materials. Cell culture reagents were freshly prepared in the core facility of the Institute of Cancer Research by using components purchased from Sigma Aldrich. The human breast adenocarcinoma cell line MCF7 was obtained from Interlab Cell Line Collection (ICLC, Genoa) and was grown in DMEM high glucose supplemented with 10% fetal bovine serum in a humidified incubator at 37 °C with a 5% CO_2 atmosphere**.**

2.6.2 Cytotoxicity tests in cancer cell lines (MTT assay). To determine the impact of the new nanocarriers on cell viability of MCF7 cells, 10^5 cells/mL were plated on 96-well plates (100 μL/well) and allowed to recover for 24 h. Then, cells were exposed to the test drugs with the different concentrations (from 0.05 to 0.0001 mg/mL) for 72 h. Anticancer activity was measured by the 3-(4,5-dimethylthiazol-2-yl)-2,5-diphenyltetrazolium bromide (MTT)-based vitality assay (EZ4U; Biomedica, Vienna, Austria) following the manufacturer's recommendations. Cytotoxicity was calculated using the Graph Pad Prism software (using a point-to-point function) and was expressed as EC50 values calculated from full dose–response curves (drug concentrations inducing a 50% reduction of cell number in comparison to untreated control cells cultured in parallel).

2.6.3 Flow cytometry analysis. Cells were incubated with QD@SiO_2–NH_2, QD@SiO_2–TA6 or QD@SiO_2–MLP66 NPs (0.010 mg/mL) for different time point (3 h, 5 h and 24 h) at 37 °C. At the end of the incubation period, cells were washed twice with phosphate-buffered saline (PBS), detached with Trypsin/EDTA (freshly prepared in the core facility of the Institute of Cancer Research, by using components purchased from Sigma Aldrich) for 10 min at 37°C, centrifuged at 1200 rpm for 5 min and re-suspended in 250 μL of PBS. The fluorescence was recorded using a FACS Calibur (Becton Dickinson, Palo Alto, CA) with a 585 nm band-pass filter. For each analysis,

10,000 events were collected and analyzed by ModeFit software (Becton Dickinson and Company, New York, USA).

2.6.4 Confocal microscopy analysis. For experiments on live cells, 10^5 cells were grown on sterile μ-Slide 8 Well Glass Bottom (Ibidi) and treated with QD@SiO_2–NH_2, QD@SiO_2–TA6 or QD@SiO_2–TA6 NPs for 24 h followed by **NO1** or **F412** treatment for 45 min, and then live cells were imaged with a Zeiss LSM 700 Olympus (Carl Zeiss AG, Oberkochen, Germany). For each experimental point, a minimum of three microscopic fields was examined. For experiments on fixed cells, 10^5 cells were grown on sterile microscope slides with removable chambers, rinsed and fixed with 4% w/v paraformaldehyde for 15 min, then rinsed and permeabilized with 0.5% triton-X 100 for 20 min. The samples were then washed with PBS and stained with QD@SiO_2–NH_2 or QD@SiO_2–TA6 or QD@SiO_2–MLP66 NPs (0.010 mg/mL) for 24 h. After washing with PBS, samples were incubated with DAPI (Sigma Aldrich) for 10 min and then washed. The coverslips were mounted with 6 μL of Vectashield Mounting Medium and examined with a Zeiss LSM 700 Olympus (Carl Zeiss AG, Oberkochen, Germany). For each experimental point, a minimum of three microscopic fields was examined.

2.6.5 Live cell microscopy analysis. 10^5 cells were grown on sterile μ-Slide 8 Well Glass Bottom (Ibidi) and treated with QD@SiO_2–NH_2, QD@SiO_2–TA6 or QD@SiO_2–MLP66 NPs (0.010 mg/mL) alone or in combination with F412 (10 μM). QD@SiO_2 NPs were added 2 h before F412. The imaging started after the addition of the green-emitting compound using Nikon eclipse Ti-e fluorescence microscope with a sCMOS pco.edge camera (Nikon Instruments Europe B.V., Amsterdam, Netherlands).

3. Results and Discussion

Silica-coated luminescent QDs were used as robust inorganic platforms to conjugate two structurally different sigma-2 receptor ligands, namely TA6 and MLP66, here proposed as sigma-2 receptor ligands, in order to generate a luminescent nanoparticle-based optically traceable tool for sigma-2 receptor targeting. A scheme depicting the steps leading to silica-coated luminescent QD conjugated with TA6 or MLP66 ligands is reported in **Chart 1**.

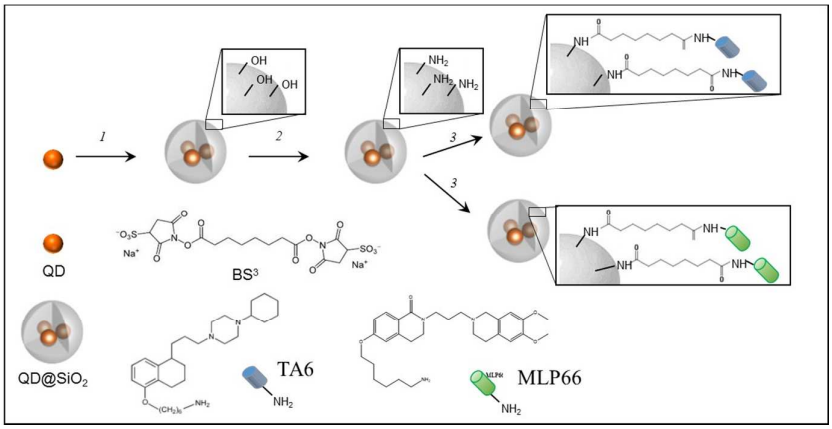

Chart 1. Scheme of the synthetic path for silica-coated QDs functionalization with sigma-2 receptor ligands. QDs are coated with a silica shell by means of a microemulsion approach (Step 1), functionalized with amine groups, through a reaction with 3-(aminopropyl)trimethoxysilane in aqueous ammonia solution (Step 2), and further conjugated to sigma-2-receptor ligands (TA6 or MLP66) by cross coupling reaction mediated by the bis(sulfosuccinimidyl)suberate (Step 3). See experimental section for details.

The proposed hybrid nanostructures aim at ingeniously combining the optical properties of QDs with the high affinity and selectivity for sigma-2-receptors of the two purposely designed ligands, in order to fabricate efficient sigma-2 targeting luminescent probes. Although promising fluorescent molecular systems based on the 1- and PB28-structure sigma-2 affinity agonists (see Figure 1) have been already proposed as optical probe targeting the sigma-2 receptor, [49-50] they suffer from low fluorescence quantum yield (QY) (below 0.6, with higher value reached in non-polar solvent or when ligand bound hydrophobic sites). Therefore, the

replacement of the fluorescent tag with inorganic luminescent QDs will potentially bring advantages by exploiting the much more stable photophysical properties of the QDs, i.e. narrow and brighter emission, high QY, reduced photobleaching effect and longer fluorescence lifetime, which may contribute to improve sensitivity, signal to noise of the hybrid fluorescent probe for *in vitro* imaging. Encapsulation of the QDs inside the silica matrix represents a wide standing procedure to make the hydrophobic QD dispersable in aqueous media and also to overcome their limitations for application in the biological field, mainly the effect of surface modification on QD photophysical properties and the release of toxic heavy metal ions. The hydrophilicity of the silica matrix, together with its inertness, good level of biocompatibility and easy of functionalization, will provide a nanostructure with relevant colloidal stability in aqueous media and high density of covalently bound ligands, that, in principle offers multiple and simultaneous interactions with cell surface, thus resulting highly active and still selective for the optically traceable targeting of sigma-2-receptor.

3.1. Synthesis of sigma-2 receptor ligands. Two structurally different synthetic molecules are proposed as sigma-2 receptor ligands, namely TA6 and MLP66, that are 6-amino-hexyloxy derivatives of previously reported PB28 and compound 1, respectively (Figure 1A). The former is a thoroughly characterized sigma-2 receptor ligand used as a tool for sigma-2 receptor studies with its subnanomolar affinity, but no selectivity towards the sigma-1 receptor. The latter belongs to the recently developed class of sigma-2 receptor binding dihydro-(2*H*)-isoquinolin-1-one derivatives, and it is endowed with a nanomolar affinity and excellent selectivity for the sigma-2 subtype (Figure 1B). Interestingly, previous studies highlighted that the fluorescent compounds F412 and NO1, based respectively on the PB28 and compound 1 scaffold suitably conjugated with green emitting fluorophores, result excellent tools for sigma-2 receptor studies, as they could be visualized by means of flow cytometry and confocal microscopy in live cells (Figure 1B).[29, 49-50] The improved

pharmacological (Figure 1B) and fluorescent properties of the two fluorescent compounds F412 and NO1, with respect to the previously reported sigma-2 fluorescent ligands,[49] were successfully achieved in the structure of PB28 and compound 1 by replacing the methoxy group by a hexamethylenoxy chain, and thus identifying the 6-methylenes chain as an optimal spacer between the sigma-2 pharmacophore and the fluorescent moiety. According to these findings, the 6-amino-hexamethylenoxy arm was here attached at 5-position on the tetralin ring for PB28 and on 6-position of the isoquinolin-1-one for compound 1 analogue, providing also the amine group as functional group for the subsequent covalent binding of the ligand with the primary amine groups at the NP silica surface. As in F412 and NO1, derivatization of PB28 and compound 1 with a long spacer from the silica-coated QDs is expected to preserve their affinity and selectivity to sigma-2 receptors.[49-50]

A

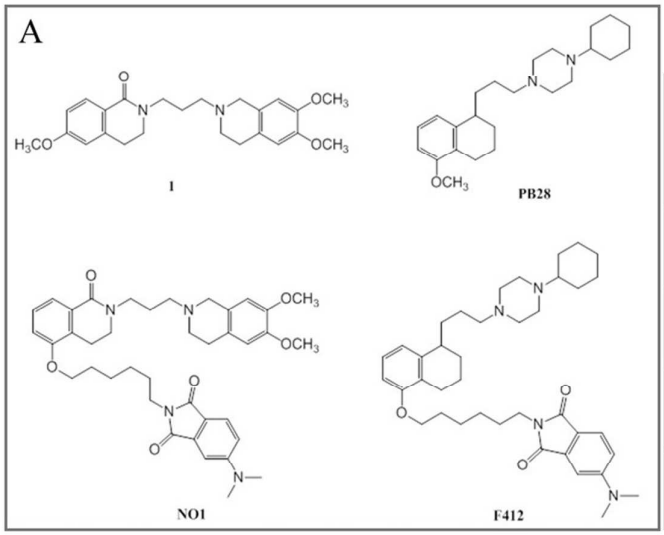

B

Compound	K_i (nM)	
	sigma-1	sigma-2
1 [a]	402	5.74
PB28 [b]	0.38	0.68
NO1 [c]	>5000	10.2
F412 [d]	5.37	6.9

Figure 1. (A) Structures of sigma-2 lead compounds (1 and PB28) and fluorescent sigma-2 ligands (NO1 and F412); (B) Table of the inhibition constants (K_i) at both sigma receptor subtypes (sigma-1 and sigma-2) for lead compounds and fluorescent ligands. *a* From ref. 45; *b* From ref. 44; *c* From ref. 50; *d* From ref. 49.

In particular, the synthesis of MLP66 is reported in **Scheme 1**, while the synthesis of TA6 was achieved through a previously reported pathway.[44] The box in the Scheme **1** reports the synthesis of the key mesylate intermediate **3**, achieved by initial protection of the amine function of the 6-amino-1-hexanol by condensation with acetonylacetone to a 2,5-dimethylpyrrole ring (2), followed by mesylation of the primary alcohol with mesyl chloride. The 6-hydroxy-3,4-dihydro-isoquinolin-(2*H*)-1-one (**4**) was obtained according to a procedure[45] previously reported for a different isomer. Benzylation of the phenolic function led to the benzyl derivative,[51] which underwent alkylation with 1-bromo-3-chloro-propane in the presence of NaH to generate intermediate **6**. Reaction of this last compound with 6,7-dimethoxytetrahydroisoquinoline led to compound **7**, whose debenzylation by H_2 in the presence of Pd on activated charcoal 10% led to the phenol intermediate **8**. Alkylation of **8** with intermediate **3** provided compound **9** that upon deprotection with NH_2OH provided the amine derivative MLP66.

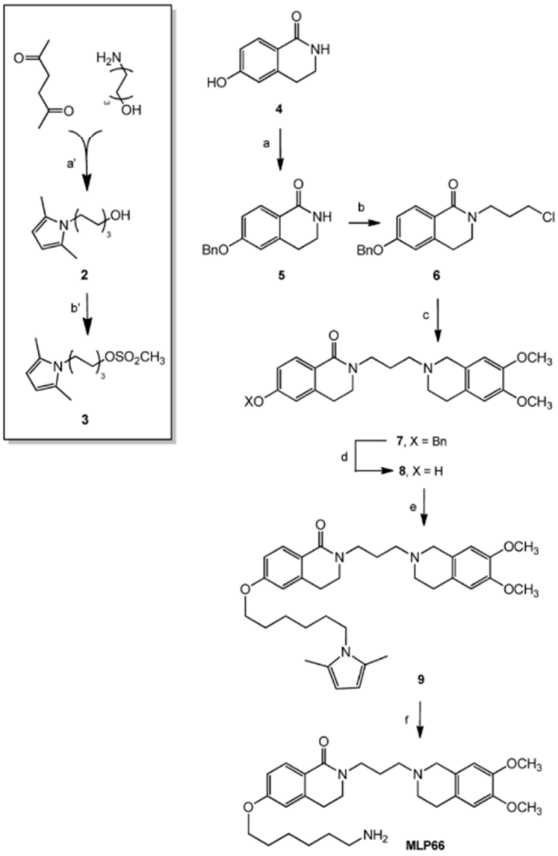

Scheme 1. Reaction scheme of the synthesis of MLP66 ligand and of the mesylate intermediate (3, left box).

While the UV-Vis absorption spectra for both the sigma-2-ligands are quite similar, characterized by an intense absorption signal below 350 nm ascribed to the aromatic π- π* transition, the spectrofluorometric investigation (λ_{ex}= 300 nm) points out the specific PL signature of TA6 (Figure 2A) and MLP66 (Figure 2B), respectively. In particular, the fluorescence spectrum of TA6 shows an emission band centered at 345 nm ascribed to the tetralin functionality (Figure 2A), while the tetrahydroisoquinoline moiety of MLP66 (Figure 2B) generates a remarkable intense band at 465 nm with a shoulder at 375 nm.

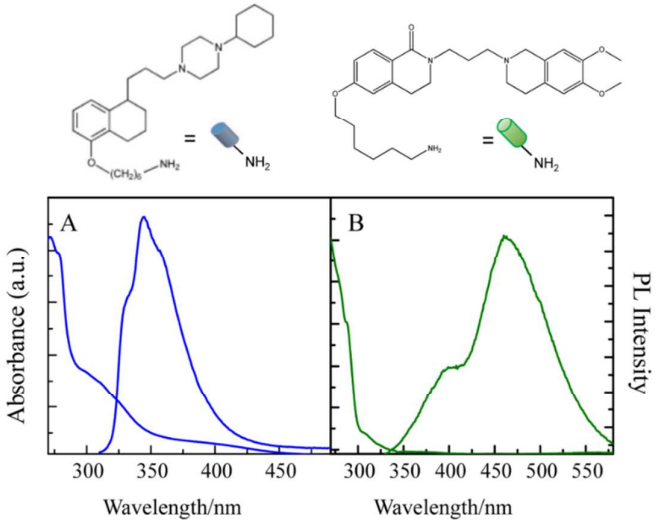

Figure 2. UV-Vis absorbance and emission spectra, λ_{ex} = 300 nm, of TA6 (A) and MLP66 (B), along with the molecular structures.

3.2 Synthesis and characterization of silica-coated QDs functionalized with sigma-2 receptor ligands

Hydrophobic, red emitting QDs (See **Figure S1**, Supporting Information for spectroscopic and morphologic characterization) were coated with a silica shell by using a microemulsion

based strategy, resulting in hydrophilic, core-shell type QD@SiO_2 NPs, with a surface that could be promptly functionalized.[13,43,47]

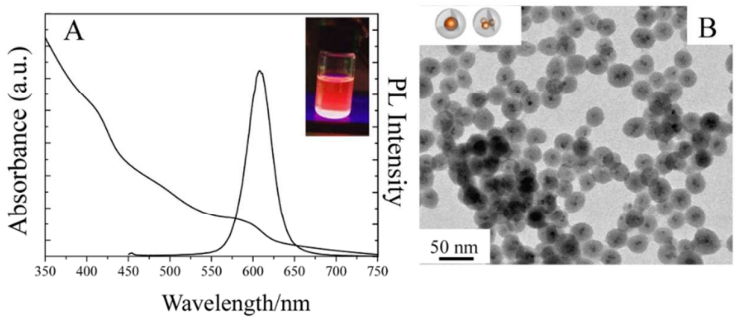

Figure 3. UV-Vis absorbance and PL emission (λex = 400 nm) spectra (A) and transmission electron micrograph (B) of silica-coated QDs.

According to this procedure, the spectroscopic properties of the QDs[48] were effectively conveyed to the resulting silica coated nanostructures, that retained the characteristic wide absorption spectrum of QDs and the narrow emission band centred at 613 nm (**Figure 3A**). In addition, TEM analysis revealed the formation of homogeneous and monodisperse core-shell structures presenting multiple QD cores embedded in a silica shell, with a spherical morphology of nearly 32 nm diameter (σ%= 15%, **Figure 3B**).

Prior to functionalization with the sigma-2 receptors ligands, primary amine (NH_2) groups were grafted onto the nanoparticle silica surface by reaction with 3-aminopropyltriethoxysilane, thus providing effective anchor sites for their subsequent covalent binding to the primary amine groups present in the two distinct ligand structures (Chart 1). TA6 and MLP66 were covalently anchored to the silica surface, in the presence of BS^3, as shown in **Figure 4**, where the characteristic emission bands for the two ligands (Figure 4 A1, B1, λ_{ex} = 300 nm) are clearly visible together with the PL fingerprint of the QDs (Figure 4 A2, B2, λ_{ex} = 400 nm), thus clearly indicating the successful conjugation of the ligands onto the luminescent NP silica surface. The emission intensity characteristic of the

two sigma-2 receptors ligands (Figure 4 A1 and B1) conjugated to luminescent silica-based NPs, allowed to estimate the concentration of each conjugated ligand in the sample, as described in the experimental section. Starting from 0.5 mg/mL of QD@SiO_2-NH_2 NPs suspension containing 2 µmol of NH_2 groups, 8.0 µg/mL (± 0.5 µg/mL) and 10.0 µg/mL (± 0.5 µg/mL) for TA6 and MLP66 ligand, respectively, were estimated.

A mixture containing amine functionalized silica-coated QDs and the free sigma-2 receptor ligands was incubated, under the same experimental conditions for conjugation reaction but without any linker, in order to demonstrate that no PL contribution arises from non-specific absorption of the two ligands at the surface of QD@SiO_2-NH_2 NPs. Indeed, any PL feature characteristic of the two ligands was observed in the emission spectrum of the purified mixture, thus indicating that the PL signals of the two ligands in the corresponding sample spectrum can be detected only thank to their covalent conjugation with amine groups at NP surface which occurs in the presence of crosslinking agents (see Supporting Information, **Figure S2**).

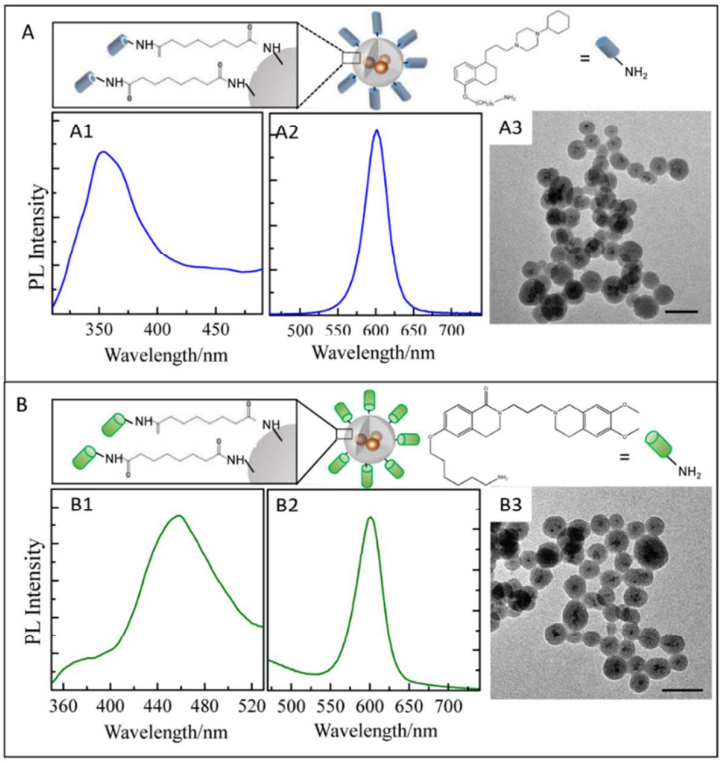

Figure 4. Sketches of the QD@SiO_2-NH_2 NPs functionalized with TA6 (Panel A) and MLP66 (Panel B) along with the corresponding fluorescence spectra (λex= 300 nm, A1, B1; λex= 400 nm, A2, B2) and TEM micrographs (A3, B3).

The retention of the peculiar optical properties of luminescent QDs can be unequivocally confirmed. The slight decrease observed in the absolute PL QY of the colloidal nanostructures dispersed in aqueous solution and measured at 400 nm (nearly 8% and 7%, for the nanostructure conjugated with MLP66 and TA6, respectively) with respect to the QY of the *as-synthesized* QDs (nearly 11%) can be reasonably ascribed to the change in the surface chemistry upon functionalization reaction and dispersant media (DMSO or water compared to the pristine hexane). Interestingly, these QY values for the MLP66- and TA6-conjugated luminescent silica-based nanostructures are significantly higher than those recorded for the overall so far reported organic sigma-2- targeting fluorescent ligands (that show an extremely low QY value in aqueous solutions,[49,50]) highlighting the promising impact of the prepared hybrids nanostructures as efficient nanoprobes for the optically traceable sigma-2 receptor targeting.

In addition, the morphological investigation of the two luminescent nanostructured conjugates was carried out by means of Transmission Electron Microscopy (TEM), Dynamic Light Scattering (DLS) analysis and ζ-potential measurements, since cellular uptake, membrane adsorption, membrane transport, as well as the fate of the NPs in the cell strongly depend on NP size, morphology and surface charge.

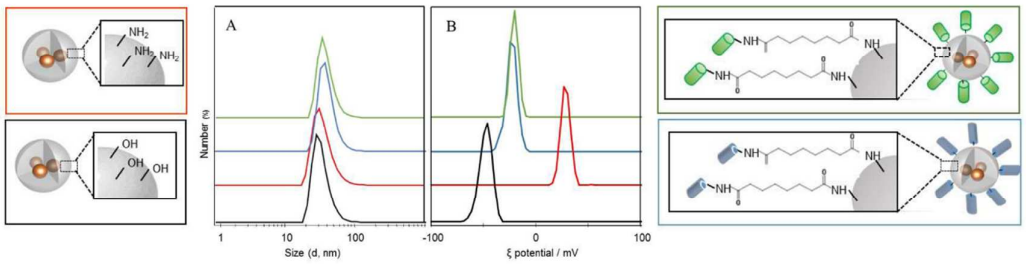

Figure 5. Size distribution obtained by DLS (A) and ζ-potential measurements (B) of QD@SiO_2 NPs (black line), amino functionalized QD@SiO_2 NPs (red line), MLP66-conjugated QD@SiO_2 NPs (green line) and TA6-conjugated QD@SiO_2 NPs (blue line), along with a sketch of the silica surface.

No significant changes in the silica-based NP morphology and in their average size were detected by TEM analysis after conjugation with the two different ligands (Figure 3 A3, B3), resulting in NPs of nearly 33 nm (σ% = 16%, Figure 4A3) and 32 nm (σ% = 15%, Figure 4 B3).

DLS analysis and ζ-potential measurements were performed to record hydrodynamic diameter and surface charge density of the luminescent QD@SiO_2 NPs, at each functionalization steps, starting from the *"as synthesized"* QD@SiO_2 NPs, to amine-functionalized QD@SiO_2 NPs, and finally to MLP66- or TA6-conjugated QD@SiO_2 NPs (**Figure 5**). DLS analysis clearly indicated, for each step, a monomodal size distribution, thus suggesting that no aggregation phenomenon of silica-based nanostructure occurs in aqueous medium. In particular, average diameters of 36 (PDI 0.261 ± 0.016), 37 (PDI 0.169 ± 0.019), 41 (PDI 0.341 ± 0.025) and 43 nm (PDI 0.225 ± 0.011) were recorded for *"as synthesized"* QD@SiO_2 NPs, amine-functionalized QD@SiO_2 NPs, TA6-conjugated QD@SiO_2 NPs and MLP66-conjugated QD@SiO_2 NPs, respectively. While no significant change in hydrodynamic diameter was observed passing from QD@SiO_2 NPs to amine functionalized QD@SiO_2 NPs, a slightly increase was recorded after silica NP conjugation with MLP66 or TA6 (Figure 5A). The size measured for sigma-2 receptor ligand conjugated-QD@SiO_2 NPs with the TEM analysis (33 and 32 nm for TA6 and MLP66 conjugated nanostructures, respectively, Figure 4) differed from the DLS measurements, being TEM observation, in the here tested experimental conditions, able to detect only the inorganic domain of the hybrid conjugated nanostructure. Conversely, the higher hydrodynamic diameter values resulting from the DLS investigation,

(namely 41 and 43 nm for TA6-conjugated QD@SiO_2 NPs and MLP66-conjugated QD@SiO_2 NPs, respectively, Figure 5A blue and green line), resulted, beside to the inorganic component, from the presence of the MLP66- or TA6-linked to NP surface, the hydration shell, and also the excess of counter ions.

ζ-potential measurements provided insights on the colloidal stability, as well as on the surface charge of the luminescent NPs at each step of the functionalization process. Upon grafting the amine groups, the negatively charged QD@SiO_2 NPs (-45.0 ± 2.0 mV, Figure 5B black line) become positive (28.6 ± 0.3 mV, Figure 5B red line), in agreement with the literature reported values.[17] Further conjugation with each of the two sigma-2 receptor ligands results in an average ζ-potential value of -20.0 ± 0.7 mV and -19.4 ± 0.8 mV for TA6 (Figure 5B, blue line) and MLP66 (Figure 5B, green line), respectively. The less positive values of QD@SiO_2 NPs functionalized with the sigma-2 receptors ligands, with respect to that of the amino functionalized sample, can be ascribed to the decrease of the amount of the free amino groups present at the surface. In details, the functionalization with either TA6 or MLP66 induces a partial charge neutralization, thanks to the formation of a covalent bond between the surface amine groups and the targeting moiety, mediated by the BS^3 spacer. Such an evidence further confirmed the success of the conjugation reaction.

3.3 Cell viability

The two types of QD@SiO_2 NPs conjugated with TA6 and MLP66 (QD@SiO_2-TA6 and QD@SiO_2-MLP66 NPs) and the unconjugated QD@SiO_2-NH_2 NPs were studied in human breast adenocarcinoma cells (MCF7). This cell type was selected, as previously and thoroughly characterized, for the presence of sigma-2 receptor, thus resulting in a well-established model for sigma-2 receptor studies.[50, 52] As a first step, the cytotoxic activity of QD@SiO_2 NPs was evaluated after long-term exposure (72 hours).

The experimental data indicated that the QD@SiO_2-MLP66 (EC_{50} = 0.007 mg/mL ±0.001, **Figure 6A** green line) and QD@SiO_2-TA6 (EC_{50} = 0.008 mg/mL ±0.001, **Figure 6A** blue line) NPs resulted in a slightly higher toxicity in MCF7 cells than the bare, unconjugated, QD@SiO_2-NH_2 NPs (EC_{50} = 0.015 mg/mL ±0.001 **Figure 6A** red line), due to the presence of the sigma-2 receptor-targeting moiety on the conjugated NP surface, as expected. Indeed, although mechanisms underlying cell death are not fully disclosed, inhibition of the sigma-2 receptor has been reported to result in caspase-dependent and/or caspase-independent apoptosis, lysosome leakage, cathepsin activation, autophagy and oxidative stress.[53]

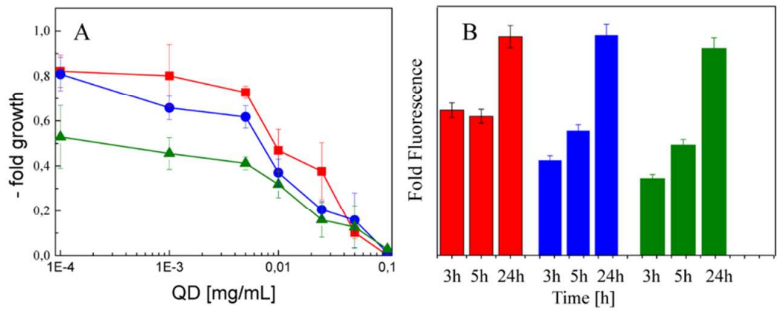

Figure 6. (A) Concentration–cell viability profiles for MCF7 cancerous cells after 72 h of incubation with QD@SiO_2-NH_2 (red line and symbol), QD@SiO_2-TA6 (blue line and symbol) and QD@SiO_2-MLP66 (green line and symbol) NPs. Each point represents a mean value of three independent experiments. (B) MCF7 cell uptake by flow cytometry analysis versus time after 3 h, 5 h or 24 h.

According to the results obtained from cytotoxicity assay, the concentration of 0.010 mg/ml was selected and used for all tested NPs (QD@SiO_2-NH_2, QD@SiO_2-MLP66 and QD@SiO_2-TA6 NPs), to perform flow cytometry, confocal, as well as live cell microscopy experiments. At this concentration, the sigma-2 targeted nanosystems have a concentration of nearly 500 nM of sigma-2 receptor affinity ligands.

3.4 Flow cytometry investigation

The fluorescence signals originated from internalized luminescent NPs allowed to quantitatively evaluate their cell uptake at three different incubation times. In particular, MCF7 cell lines were treated with QD@SiO_2-NH_2, QD@SiO_2-MLP66 or QD@SiO_2-TA6 NPs, at a concentration of 0.010 mg/mL, for 3 h, 5 h or 24 h (**Figure 6B**). The obtained results clearly indicated cellular uptake of targeted and non-targeted luminescent silica-based NPs, thus highlighting the time-dependence of the extracellular membrane crossing and penetration.

While QD@SiO_2-NH_2 NPs (Figure 6B, red bars) could already be detected inside the cells after 3 h, the conjugated QD@SiO_2-TA6 (Figure 6B, blue bars) and QD@SiO_2-MLP66 (Figure 6B, green bars) NPs took longer to enter the cells. This behaviour can be explained by assuming different pathways involved for the cell internalization for the targeted and non-targeted NPs.

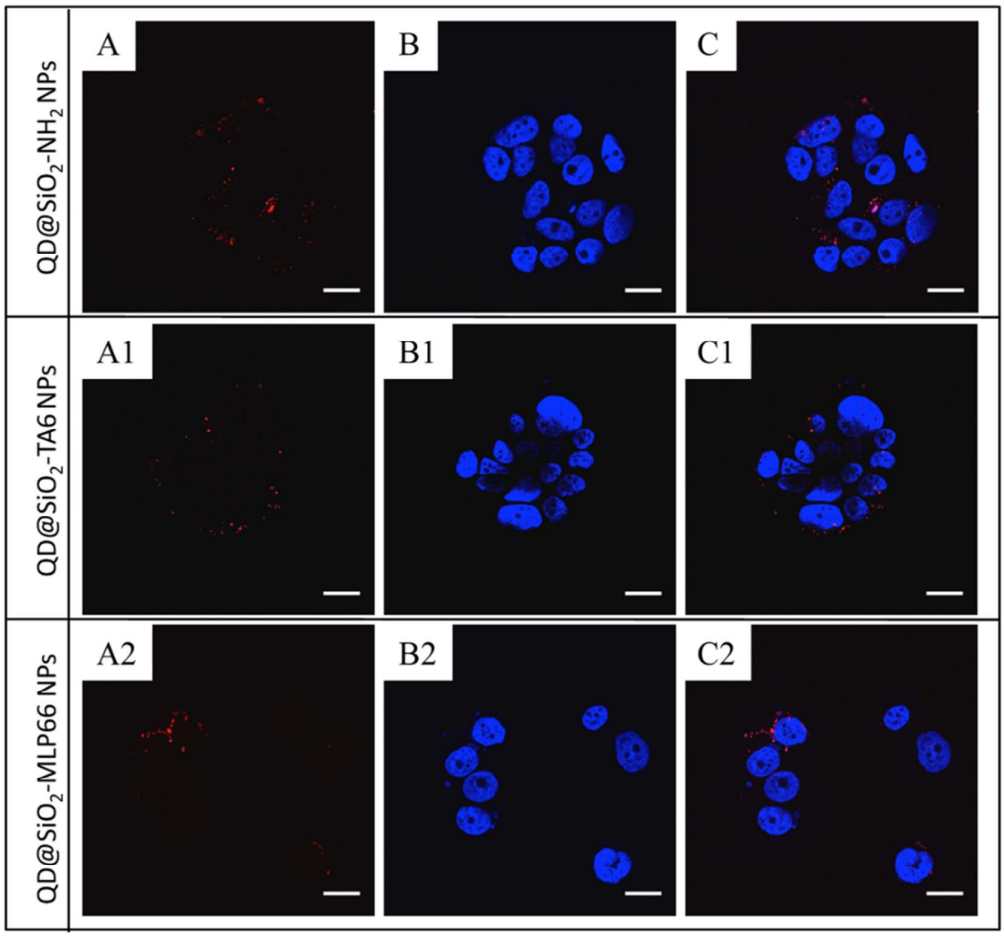

Figure 7. Representative single central confocal slice of fixed MCF7 cells imaged incubated with QD@SiO_2-NH_2 (A-C), QD@SiO_2-TA6 (A1-C1) and QD@SiO_2-MLP66 (A2-C2) NPs for 24 h and stained with DAPI. Red (A, A1, A2), blue (B, B1, B2) and overlays detection channel (C, C1, C2). Scale bar 20 nm.

The surface charge shift from positive to negative values passing from QD@SiO_2-NH_2 to QD@SiO_2-MLP66 or QD@SiO_2-TA6 NPs, respectively, may contribute to explain their different behaviour in the cell internalization process. NPs smaller than 50 nm in diameter and >10 mV surface charge were reported to undergo an enhanced cellular internalization through a nonspecific process, namely adsorptive endocytosis,[54] and that cellular uptake of anionic NPs can be slower than that of cationic NPs.[55]

Indeed, as electrostatic interactions are considered important in NP−cell interaction, it is reasonable to assume that the internalization of positive charges at the surface of QD@SiO_2-NH_2 (with ≤ 50 nm size and >10 mV surface charge) can be promoted by binding to the large negatively charged domains which are present at the cell surface thus initiating their rapid uptake, mainly via predominant clathrin-mediated endocytosis.[54,56] Conversely, the observed cellular uptake of negatively charged and targeted QD@SiO_2-MLP66 or QD@SiO_2-TA6 NPs could involve their adsorption to the few cationic sites on the cell surface. Importantly, a receptor-mediated endocytosis cannot be completely excluded, since previous studies proved that sigma-2 receptors exist in lipid rafts, which are organized microdomains in cell membranes, largely found in the plasma membrane.[53]

Therefore, according to the experimental findings obtained by flow cytometry measurements, the confocal microscopy experiments were subsequently performed after 24 h incubation (**Figure 7**).

3.5 Confocal Microscopy Investigation

Here MCF7 cells, after 24 h incubation with the 0.010 mg/mL of red-emitting QD@SiO_2-NH_2 (Figure 7A-C), QD@SiO_2-TA6 (Figure 7A1-C1) and QD@SiO_2-MLP66 (Figure 7A2-C2) NP samples, were fixed and stained with DAPI, (blue-emitting dye, generally used to stain nuclei of fixed cells, since it is cell-impermeant) to attain preliminary information on the intracellular distribution of the nanostructures. Images at different focal planes were recorded in order to render and visualize the entire sample volume. In particular, ten “Z stacks” were registered by incrementally stepping through the fixed cell samples using a focal drive, and in Figure 7 the central stack acquired for the fixed MCF7 cells incubated with the QD@SiO_2-NPs (red) and stained with DAPI (blue) are reported. The analysis revealed that red-emitting spots are clearly visible in the red detection channel and are ascribed to the QD@SiO_2 nanostructures (Figure 7 A, A1, A2). The merge pictures (Figure 7 C, C1, C2), that reports the

overlapping of the red detection channel with the blue ones used to visualize the DAPI (Figure 7 B, B1, B2), show the red emitting spots close to the blue-emitting features (nuclei). The image confirms the amine- and sigma-2 ligands-functionalized nanostructures uptake, in agreement with the flow cytometry experiments, although co-localization of the two targeted luminescent nanostructures in the nucleus was not observed, proving that none of the three tested silica nanoparticles were localized in the nuclei. In order to investigate, whether the targeted NPs co-localize with sigma-2 receptor, co-localization experiments by co-incubated 0.010 mg/mL of functionalized QD@SiO_2 NPs and 10 μM of green-emitting sigma-2 receptor agonist **NO1** (**Figure 8**, experiments were also performed with **F412** at 10 μM, data not shown) were conducted using live MCF7 cells. Confocal microscopy imaging in live cells represent an imaging modality able to give a more accurate picture of the intracellular location of QD@SiO_2 NPs.

While the more diffusible small fluorescent sigma-2 ligand **NO-1** thoroughly distributes in the cytoplasm in accordance with the sigma-2 receptor localization at diverse cytoplasmic organelles, the rather large QDs appear to be less distributed.[53] In addition, the overlay channels reported in Figure 8 C-C2 reveal that while for QD@SiO_2-NH_2 no co-localization with **NO1** occur (Figure 8C, see also Figure S3a in the Supporting Information), a not negligible number of yellow spots ascribed to co-localization of red-emitting QD@SiO_2-TA6 or QD@SiO_2-MLP66 NPs with green-emitting **NO1** are clearly visible in Figure 8C1-C2 (see also Figure S3b-c in the Supporting Information). This highlights a similar intracellular fate after the cell internalization of both the small fluorescent sigma-2 ligand and targeted luminescent NPs, finally supporting their comparable targeting affinity for sigma-2 receptor.

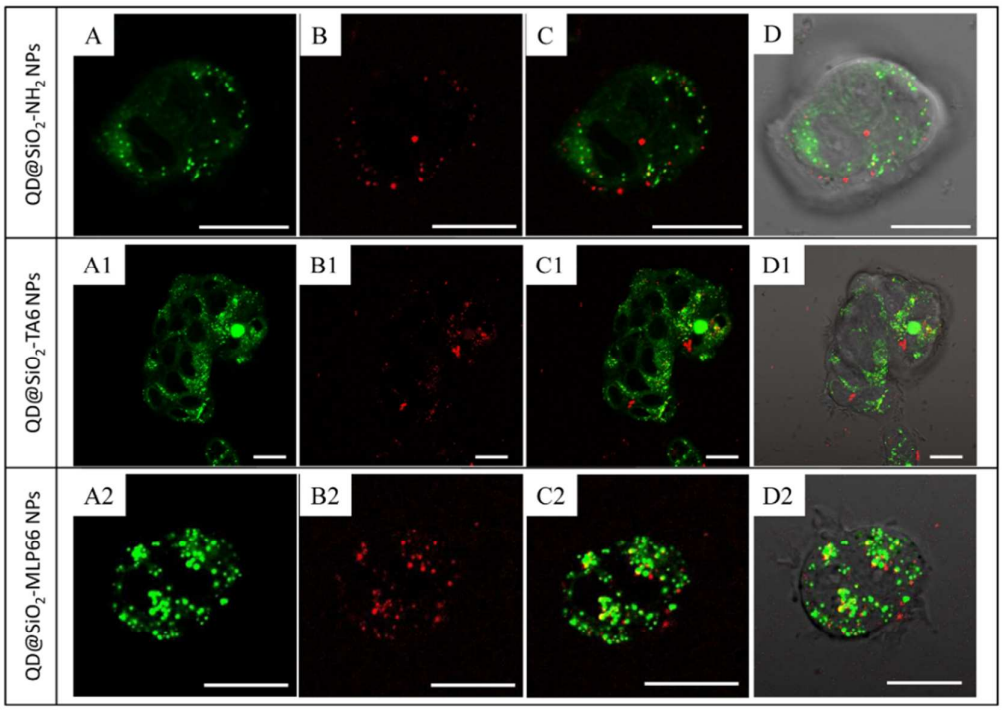

Figure 8. Confocal microscopy analysis showing live MCF7 cells stained with the fluorescent sigma-2 receptor ligand NO1 (10 μM, green), and QD@SiO_2-NH_2 (A-D), QD@SiO_2-TA6 (A1-D1) or QD@SiO_2-MLP66 (A2-D2) NPs (0.010 mg/ml, red). Green (A, A1, A2), red (B, B1, B2) along with the overlay (C, C1, C2) and bright field detection channels (D, D1, D2). Scale bar=20 μm. Each image is representative of one experiment out of three.

The absence of more important portions of co-localization may be justified by the different kinetics of the small fluorescent ligand saturating the sigma-2 receptors. In addition, it is worth to note that while NO1 sigma-2 ligand used for incubation with MCF7 cells in live cells experiments had a concentration of 10 μM, in the case the targeted NPs (QD@SiO_2-TA6 and QD@SiO_2-MLP66) a concentration of 0.010 mg/mL was exploited, which corresponds to a ligand concentration at NP surface of nearly 500 nM (as estimated from the spectroscopic characterization). This means that the NO1 agonist, used for cells experiments, was about 20 times more concentrated than the ligands, conjugated to NP silica surface. While the

significant excess of more diffusive NO1 small molecules with respect to ligand concentration in the nanosystems may account for a wider spread in the intracellular environment. However, the two ligands delivered by means of luminescent silica nanoparticles, are also able to co-localize with the competitors, in spite of the significantly lower tested concentration. Similar results were obtained by using the small fluorescent molecules F412 (data not shown).

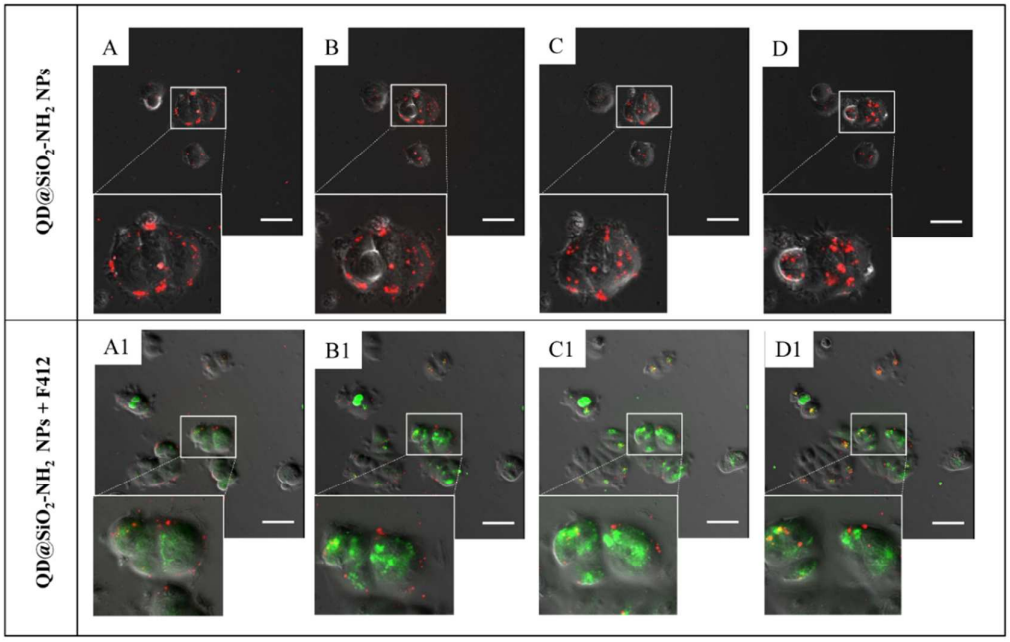

Figure 9. Live cell microscopy analysis showing MCF7 cells stained with QD@SiO_2-NH_2 NPs (0.010 mg/mL, red-emitting spots A-D) added 2 h before the fluorescent sigma-2 receptor ligand F412 (10 μM, green_emitting fluorescence A1-D1). The images were recorded after 75 min (A, A1), 3 h (B, B1), 6 h (C, C1) or 9 h (D, D1) from the addition of F412. Each image is representative of one experiment out of three. Scale bar 1 μm

3.6 Live cell microscopy investigation

Live cell microscopy studies allow to conveniently investigate the treated cells in real time by taking pictures every 10 min. According to the results obtained by flow cytometry, while QD@SiO_2-NH_2 was rapidly internalized into MCF7 cells (3 h,

Figure 9B, See Supporting Information Movie 1), QD@SiO_2-TA6 (**Figure 10 A-D**, See Supporting Information Movie 2) and QD@SiO_2-MLP66 (**Figure 11 A-D**, See Supporting Information Movie 3) NP uptake was distinctly slower with the first QD@SiO_2 NPs entering cells after at least 6h (Figure 10C, 11C). **F412** or **NO1** rapidly enter cells (within 75 min) while the QD@SiO_2 NPs need more time. Therefore, **F412** or **NO1** (data not shown) were added two hours after the three QD@SiO_2 NP samples were administrated, and pictures were taken immediately afterwards. Importantly, when **F412** are added to the culture medium, QD@SiO_2-TA6 or QD@SiO_2 -MLP66 NPs are no longer able to enter cells, thus creating aggregates outside the cells (red emitting clusters, Figure 10 A1-D1 and 11 A1-D1, See Electronic Supplementary Information Movie 4-5), while **F412** immediately permeate the cells (green emitting clusters, **Figure 10 A1-D1** and **Figure 11 A1-D1**).

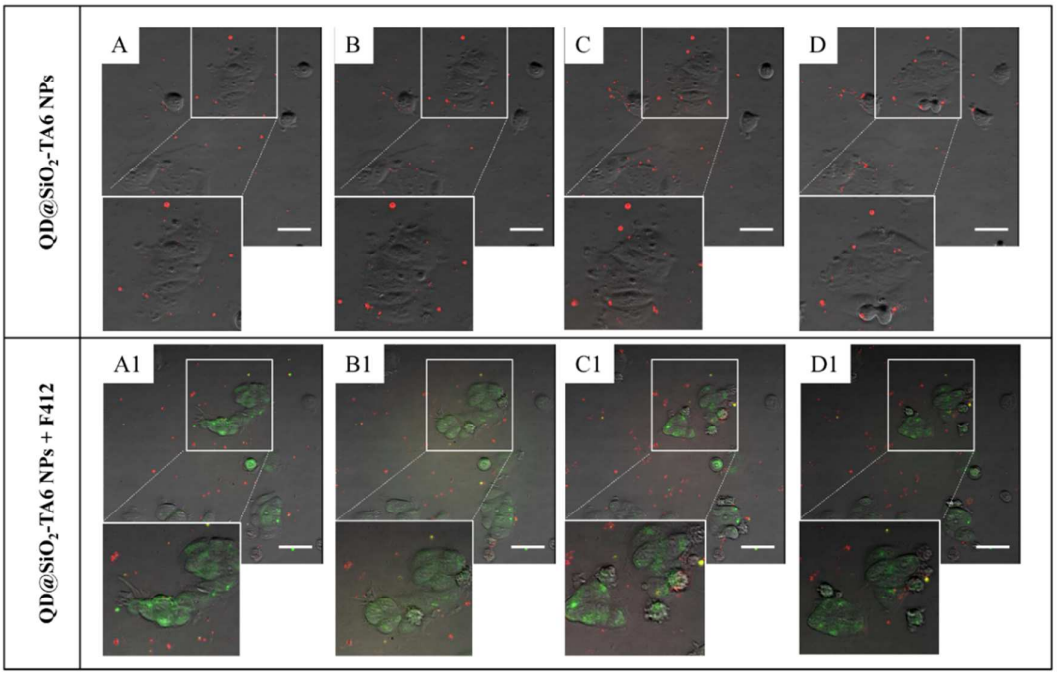

Figure 10. Live cell microscopy analysis showing MCF7 cells stained with QD@SiO_2-TA6 NPs (0.010 mg/mL, red emitting spots, A-D) added 2 h before the fluorescent sigma-2 receptor ligand F412 (10 µM, green emitting spots, A1-D1). The images were recorded after

75 min (A, A1), 3 h (B, B1), 6 h (C, C1) or 9 h (D, D1) from the addition of F412. Each image is representative of one experiment out of three. Scale bar 1 μm.

On the other hand, application of **F412** does not disturb QD@SiO_2-NH_2 NP entrance into cells, with nanostructures (red emitting clusters Figure 9A1-D1, See Supporting Information Movie 6) and small molecules (green emitting clusters **Figure 9A1-D1**) passing the cell membranes and distributing into cells. Similar results were achieved with NO1 (data not shown).

Therefore, live cell microscopy investigation showed that when the fluorescent small sigma-2 ligands are applied right before QD@SiO_2 -TA6 or QD@SiO_2 -MLP66 NPs start entering the cells, they rapidly enter MCF7 cells (as previously shown[49]) and, at the concentration used, they completely hamper the entrance of the fluorescent QD@SiO_2 -TA6 and QD@SiO_2 –MLP66 nanostructures, assumingly competing for the sigma-2 receptor-mediated entrance at plasma membrane level and supporting the hypothesis that their cell internalization may be allowed by sigma-2 receptor localized on the plasma membrane after receptor binding as previously shown.[53]

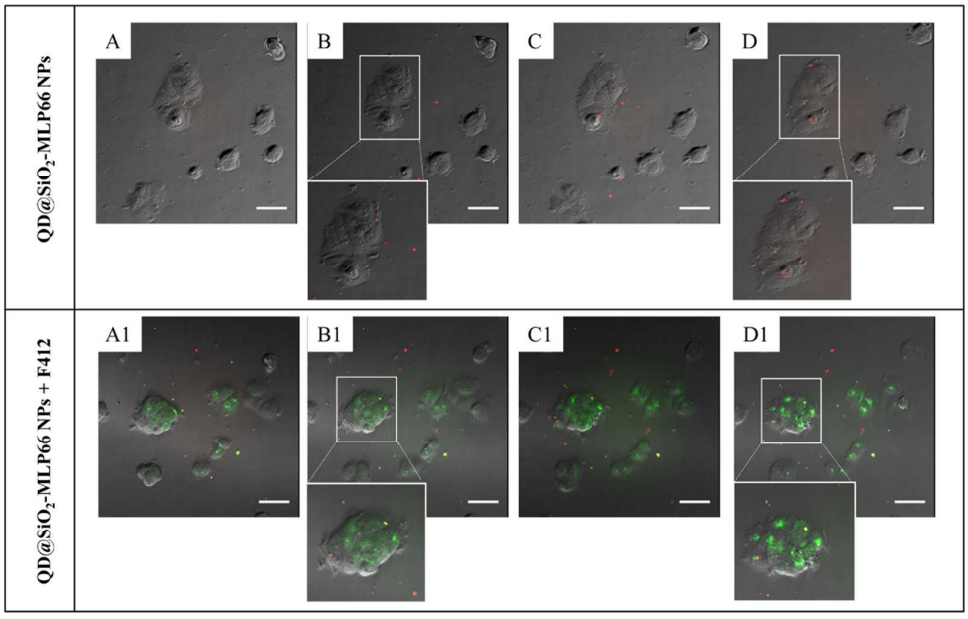

Figure 11. Live cell microscopy analysis showing MCF7 cells stained with QD@SiO_2-MLP66 NPs (0.010 mg/mL, red emitting spots A-D) added 2 h before F412 (10 μM, green emitting spots, A1-D1). The images were recorded after 75 min (A, A1), 3 h (B, B1), 6 h (C, C1) or 9 h (D, D1) from the addition of F412. Each image is representative of one experiment out of three. Scale bar 1 μm.

However, incubation of cells with sigma-2 ligand-functionalized QD@SiO_2 NPs together with **F412** or **NO1** for a longer time than 12 h resulted in a change of cell morphology. Such an evidence of toxicity may be accounted for by the effect of **F412** and **NO1** in addition to the repeated exposure of the cells to illumination from fluorescence imaging.

4. Conclusion

The work reports the design, synthesis and characterization of two optically traceable sigma-2-targeting nanoprobes, based on two synthetic sigma-2 ligands, TA6 and MLP66, bound at the surface of QD@SiO_2 NPs. The QD@SiO_2-TA6 and QD@SiO_2-MLP66 NPs, respectively, show more stable photophysical properties and improved stability of ligands in aqueous media compared to the reported luminescent molecular ligands, namely F412 and NO1, based on the same PB28 and 1- structure, previously used for the sigma-2 receptor targeting. In addition, the nanosystems reveal their ability to be cell internalized and delivered to the sigma-2 receptor, as proven by the *in vitro* experiments in MCF7 cells, here selected due to their sigma-2 receptor overexpression.

Spectroscopic, morphological, colloidal stability and surface chemistry analysis, carried out by complementary techniques (TEM, DLS and ζ-potential measurements), provided fundamental information of the optical properties, size regime and surface properties of the

nanosystems, that played a crucial role in the nanostructures cell uptake. The exploitation of inorganic QDs as fluorescent tag bring bright and narrow emission band as well as very good resistance to photobleaching, and a sigma-2 targeted nanosystem fluorescent QY that reached up to 8% in aqueous media. Moreover, the poor solubility in aqueous buffer of the free bases NO1 and F412 were overcome by anchoring the MLP66 and TA6 ligands to the hydrophilic silica shell that confers better colloidal stability of ligands in aqueous solution and multivalence, arising from the conjugation of multiple ligands to silica surface.

In vitro experiments based on flow cytometry and confocal fluorescent microscopy on fixed and/or live MCF7 tumour cells performed by incubating no targeted (QD@SiO_2-NH_2) and targeted (QD@SiO_2-TA6 and QD@SiO_2-MLP66) NPs demonstrated the cellular uptake of the nanostructures in a time-dependent manner. Moreover, co-incubation of highly diffusible F412 small fluorescent sigma-2 receptor ligands, proved the ability to partially co-localize at subcellular level in the case of QD@SiO_2-TA6 and QD@SiO_2-MLP66 NPs, in spite of the low concentration of the sigma-2 ligands bound to the silica surface. Conversely, the non-targeted QD@SiO_2-NH_2 NPs resulted in non-specific distribution into cells. The ensemble of the obtained results highlighted that the proposed sigma-2-targeted nanostructures can be selectively delivered to the sigma-2 receptors in the tumour cells, thus holding a great promise for the evaluation of the *in vitro* biological behaviour of the sigma-2 receptor ligands. Further insights on *in vitro* interactions between sigma 2 receptor and its specifically designed ligands are expected to be essential for the future development of efficient nanosystems able to *in vivo* target the sigma-2 proteins, for their use in the oncology field, not only for diagnostic but also for therapeutic purposes.

Supporting Information. Figure S1: UV-Vis absorption and fluorescence spectra, TEM micrograph and corresponding statistical analysis of as-synthesized QDs; Figure S2: Fluorescence spectra of QD-TA6; Figure S3 Overlay detection channel of confocal microscopy analysis showing live MCF7 cells co-incubated with the fluorescent sigma-2

receptor ligand NO1 and red emitting QD@SiO_2-NH_2 QD@SiO_2-TA6 and QD@SiO_2-MLP66 NPs.

Acknowledgements

The work has been supported by FIRB Futuro in Ricerca [RBFR122HFZ], Nanomax-integrable sensors for pathological biomarkers diagnosis (N-CHEM) and NANOfotocatalizzatori per un'Atmosfera più PULita (NANOAPULIA) projects and the Apulia Regional Projects RELA-VALBIOR POR FSE 2007-20013 and Laboratorio Regionale di Sintesi e Caratterizzazione di Nuovi Materiali Organici e Nanostrutturati per Elettronica, Fotonica e Tecnologie Avanzate. The Inter-University Consortium for Research on the Chemistry of Metal Ions in Biological Systems (C.I.R.C.M.S.B.) is gratefully acknowledge for their financial support.

References

1. Siegel, R. L.; Miller, K. D.; Jemal, A. Cancer statistics, 2017. *CA Cancer J. Clin.* **2017,** *67,* 7–30.
2. Liang, X.; Chen, C.; Zhao, Y.; Wang, P. C. Circumventing tumor resistance to chemotherapy by nanotechnology. *Methods Mol. Biol.* **2010**, *596*, 467–488.
3. Davis, M. E.; Chen, Z. G.; Shin, D. M. Nanoparticle therapeutics: an emerging treatment modality for cancer. *Nature Reviews Drug Discovery* **2008**, *7*, 771–782.
4. Sanna, V.; Pala, N.; Sechi, M. Targeted therapy using nanotechnology: focus on cancer. *Int. J. Nanomedicine* **2014**, *9*, 467–483.
5. Yu, M. K.; Park, J.; Jon, S. Targeting Strategies for Multifunctional Nanoparticles in Cancer Imaging and Therapy. *Theranostics* **2012**, *2*, 3–44.
6. Lopalco, A.; Ali, H.; Denora, N.; Rytting, E. Oxcarbazepine-loaded polymeric nanoparticles: development and permeability studies across in vitro models of the blood-brain barrier and human placental trophoblast. *Int. J. Nanomedicine* **2015**, *10*, 1985–1996.
7. Dykman, L.; Khlebtsov, N. Gold nanoparticles in biomedical applications: recent advances and perspectives. *Chem. Soc. Rev.* **2012**, *41*, 2256–2282.
8. Arvizo, R.; Bhattacharya, R.; Mukherjee, P. Gold nanoparticles: opportunities and challenges in nanomedicine. *Expert Opin. Drug Deliv.* **2010,** *7*, 753–763.
9. Volkov, Y. Quantum Dots in Nanomedicine: Recent Trends, Advances and Unresolved Issues. *Biochem. Biophys. Res. Commun.* **2015**, *468*, 419–427.
10. Book Light-Responsive Nanostructured Systems for Applications in Nanomedicine, Volume 370 of the series Topics in Current Chemistry Ed. S. Sortino, *Springer International Publishing* 2016; pp 203–224.

11. Mahmoudi, M.; Sant, S.; Wang, B.; Laurent, S.; Sen, T. Superparamagnetic iron oxide nanoparticles (SPIONs): development, surface modification and applications in chemotherapy. *Advanced Drug Delivery Reviews* **2011**, *63*, 24–46.

12. Silva, A. K. A.; Espinosa, A.; Kolosnjaj-Tabi, J.; Wilhelm, C.; Gazeau, F. Medical Applications of Iron Oxide Nanoparticles, in Iron Oxides: From Nature to Applications, (ed D. Faivre), Wiley-VCH Verlag GmbH & Co. KGaA, Weinheim, Germany, 2016, doi: 10.1002/9783527691395.ch18.

13. Fanizza, E.; Urso, C.; Iacobazzi, R. M.; Depalo, N.; Corricelli, M.; Panniello, A.; Agostiano, A.; Denora, N.; Laquintana, V.; Striccoli, M.; Curri, M. L. Fabrication of photoactive heterostructures based on quantum dots decorated with Au nanoparticles. *Science and Technology of Advanced Materials* **2016**, *17*, 98–108.

14. Chen, G.; Roy, I.; Yang, C.; Prasad, P. N. Nanochemistry and Nanomedicine for Nanoparticle-based Diagnostics and Therapy. *Chem. Rev.* **2016**, *116*, 2826-2885

15. Xie, J.; Lee, S.; Chen, X. Nanoparticle-based theranostic agents. *Adv. Drug Deliv. Rev.* **2010**, *62*, 1064–1079.

16. Janib, S. M.; Moses, A. S.; MacKay, J. A. Imaging and drug delivery using theranostic nanoparticles. *Adv. Drug Deliv. Rev.* **2010**, *62*, 1052–1063.

17. Fanizza, E.; Iacobazzi, R. M.; Laquintana, V.; Valente, G.; Caliandro, G.; Striccoli, M.; Agostiano, A.; Cutrignelli, A.; Lopedota, A. A.; Curri, M. L.; Franco, M.; Depalo, N.; Denora, N. Highly selective luminescent nanostructures for mitochondrial imaging and targeting. *Nanoscale* **2016**, *8*, 3350–3361.

18. Depalo, N.; De Leo, V.; Corricelli, M.; Gristina, R.; Valente, G.; Casamassima, E.; Comparelli, R.; Laquintana, V.; Denora, N.; Fanizza, E.; Striccoli, M.; Agostiano, A.; Catucci, L.; Curri, M. L. Lipid-based systems loaded with PbS nanocrystals: near infrared emitting trackable nanovectors. *J. Mater. Chem. B* **2017**, *5*, 1471–1481.

19. Valente, G.; Depalo, N.; De Paola, I.; Iacobazzi, R. M.; Denora, N.; Laquintana, V.; Comparelli, R.; Altamura, E.; Latronico, T.; Altomare, M.; Fanizza, E.; Striccoli, M.; Agostiano, A.; Saviano, M.; Del Gatto, A.; Zaccaro, L.; Curri, M. L. Integrin-targeting with peptide-bioconjugated semiconductor-magnetic nanocrystalline heterostructures. *Nanoresearch* **2016,** *9*, 644–662.

20. Liang, J. J.; Zhou, Y. Y.; Wu, J.; Ding, Y. Gold Nanoparticle-Based Drug Delivery Platform for Antineoplastic Chemotherapy. *Curr. Drug Metab.* **2014**, *15*, 620–631.

21. Wanga, M.; Thanoua, M. Targeting nanoparticles to cancer. *Pharmacological Research* **2010**, *62*, 90–99.

22. Depalo, N.; Iacobazzi, R. M.; Valente, G.; Arduino, I.; Villa, S.; Canepa, F.; Laquintana, V.; Fanizza, E.; Striccoli, M.; Cutrignelli, A.; Lopedota, A.; Porcelli, L.; Azzariti, A.; Franco, M.; Curri, M. L.; Denora, N. Sorafenib delivery nanoplatform based on superparamagnetic iron oxide nanoparticles magnetically targets hepatocellular carcinoma. *Nano Res.* **2017**, *10*, 2431–2448.

23. Laquintana, V.; Denora, N.; Lopalco, A.; Lopedota, A.; Cutrignelli, A.; Lasorsa, F. M.; Agostino, G.; Franco, M. Translocator Protein Ligand–PLGA Conjugated Nanoparticles for 5-Fluorouracil Delivery to Glioma Cancer Cells. *Mol. Pharmaceutics* **2014**, *11*, 859–871.

24. Schmidt, H. R.; Zheng, S.; Gurpinar, E.; Koehl, A.; Manglik, A.; Kruse, A. C. Crystal structure of the human σ1 receptor. *Nature* **2016**, *532*, 527–530.

25. Colabufo, N. A.; Berardi, F.; Abate, C.; Contino, M.; Niso, M.; Perrone, R. Is the sigma2 receptor a histone binding protein? *J. Med. Chem.* **2006**, *49*, 4153–4158.

26. Xu, J.; Zeng, C.; Chu, W.; Pan, F.; Rothfuss, J. M.; Zhang, F.; Tu, Z.; Zhou, D.; Zeng, D.; Vangveravong, S.; Johston, F.; Spitzer, D.; Chang, K. C.; Hotchkiss, R. S.; Hawkins, W. G.; Wheeler, K. T.; Mach, R. H. Identification of the PGRMC1 protein complex as the putative sigma-2 receptor binding site. *Nat. Commun.* **2011**, *2*, 380.

27. Abate, C.; Niso, M.; Infantino, V.; Menga, A.; Berardi, F. Elements in support of the 'non-identity' of the PGRMC1 protein with the σ2 receptor. *Eur. J. Pharmacol.* **2015**, *758*, 16–23.

28. Chu, U. B.; Mavlyutov, T. A.; Chu, M. L.; Yang, H.; Schulman, A.; Mesangeau, C.; McCurdy, C. R.; Guo, L. W.; Ruoho, A. E. The Sigma-2 Receptor and Progesterone Receptor Membrane Component 1 are Different Binding Sites Derived From Independent Genes. *E. Bio. Medicine* **2015**, *2*, 1806–1813.

29. Pati, M. L.; Groza, D.; Riganti, C.; Kopecka, J.; Niso, M.; Berardi, F.; Hager, S.; Heffeter, P.; Hirai, M.; Tsugawa, H.; Kabe, Y.; Suematsu, M.; Abate, C. Sigma-2 receptor and progesterone receptor membrane component 1 (PGRMC1) are two different proteins: Proofs by fluorescent labeling and binding of sigma-2 receptor ligands to PGRMC1. *Pharmacol. Res.* **2017**, *117*, 67–74.

30. Alon, A.; Schmidt, H. R.; Wood, M. D.; Sahn, J. J.; Martin, S. F.; Kruse, A. C. Identification of the gene that codes for the σ2 receptor. *Proc. Natl. Acad. Sci.* **2017**, *114*, 7160–7165.

31. van Waarde, A.; Rybczynska, A. A.; Ramakrishnan, N.; Ishiwata, K.; Elsinga, P. H.; Dierckx, R. A. Sigma receptors in oncology: therapeutic and diagnostic applications of sigma ligands. *Curr. Pharm. Des*. **2010**, *16*, 3519–3537.

32. Pati, M. L.; Hornick, J. R.; Niso, M.; Berardi, F.; Spitzer, D.; Abate, C.; Hawkins, W. Sigma-2 receptor agonist derivatives of 1-Cyclohexyl-4-[3-(5-methoxy-1,2,3,4-tetrahydronaphthalen-1-yl)propyl]piperazine (PB28) induce cell death via mitochondrial superoxide production and caspase activation in pancreatic cancer. *BMC Cancer* **2017**, *17*, 51.

33. Kashiwagi, H.; McDunn, J. E.; Simon, P. O.; Goedegebuure, P. S.; Mach, R. H.; Hawkins, W. G. Selective sigma-2 ligands preferentially bind to pancreatic

adenocarcinomas: applications in diagnostic imaging and therapy. *Mol. Cancer* **2007**, *6*, 48.

34. Hornick, J. R.; Xu, J.; Vangveravong, S.; Tu, Z.; Mitchem, J. B.; Spitzer, D.; Goedegebuure, P.; Mach, R. H.; Hawkins, W.G. The novel sigma-2 receptor ligand SW43 stabilizes pancreas cancer progression in combination with gemcitabine. *Mol. Cancer* **2010**, *9*, 298.
35. ClinicalTrials.gov Identifier: NCT02284919. Imaging of In Vivo Sigma-2 Receptor Expression With [^{18}F] ISO-1 Positron Emission Tomography (PET/CT) in Primary Breast Cancer.
36. ClinicalTrials.gov Identifier: NCT02204202. Positron Emission Tomography Assessment of Acute Lung Transplant Rejection.
37. Wang, Y.; Xu, J.; Xia, X.; Yang, M.; Vangveravong, S.; Chen, J.; Mach, R. H.; Xia, Y. SV119-gold nanocage conjugates: a new platform for targeting cancer cells via sigma-2 receptors. *Nanoscale* 2012, 4, 421–424.
38. Garg, G.; Vangveravong, S.; Zeng, C.; Collins, L.; Hornick, M.; Hashim, Y.; Piwnica-Worms, D.; Powell, M. A.; Mutch, D. G.; Mach, R. H.; Hawkins, W. G.; Spitzer, D. Conjugation to a SMAC mimetic potentiates sigma-2 ligand induced tumor cell death in ovarian cancer. *Mol. Cancer* 2014, *13,* 50.
39. Hashim, Y. M.; Vangveravong, S.; Sankpal, N. V.; Binder, P. S.; Liu, J.; Goedegebuure, P.; Mach, R. H.; Spitzer, D.; Hawkins, W. G. The Targeted SMAC Mimetic SW IV-134 is a strong enhancer of standard chemotherapy in pancreatic cancer. *J. Exp. Clin. Cancer Res.* **2017**, *36*, 14.
40. Fitzgerald, K. A.; Rahme, K.; Guo, J.; Holmes, J. D.; O'Driscoll, C. M. Anisamide-targeted gold nanoparticles for siRNA delivery in prostate cancer – synthesis, physicochemical characterization and in vitro evaluation *J. Mater. Chem. B* **2016**, *4*, 2242–2252.

41. Dasargyri, A.; Hervella, P.; Christiansen, A.; Proulx, S. T.; Detmar, M.; Leroux, J. C. Findings questioning the involvement of Sigma-1 receptor in the uptake of anisamide-decorated particles. *J. Control. Release* **2016**, *224*, 229–238.

42. Latronico, T.; Depalo, N.; Valente, G.; Fanizza, E.; Laquintana, V.; Denora, N.; Fasano, A.; Striccoli, M.; Colella, M.; Agostiano, A.; Curri, M. L.; Liuzzi, M. G. Cytotoxicity Study on Luminescent Nanocrystals Containing Phospholipid Micelles in Primary Cultures of Rat Astrocytes. *PLOSOne* **2016**, *11*, e0153451

43. Corricelli, M.; Depalo, N.; Di Carlo, E.; Fanizza, E.; Laquintana, V.; Denora, N.; Agostiano, A.; Striccoli, M.; Curri, M. L. Biotin-decorated silica coated PbS nanocrystals emitting in the second biological near infrared window for bioimaging. *Nanoscale* **2014**, *6*, 7924–7933.

44. Abate, C.; Niso, M.; Lacivita, E.; Mosier, P. D.; Toscano, A.; Perrone, R. Analogues of σ Receptor Ligand 1-Cyclohexyl-4-[3-(5-methoxy-1,2,3,4-tetrahydronaphthalen-1-yl)propyl]piperazine (PB28) with Added Polar Functionality and Reduced Lipophilicity for Potential Use as Positron Emission Tomography Radiotracers. *J. Med. Chem.* **2011**, *54*, 1022–1032.

45. Abate, C.; Selivanova, S. V.; Müller, A.; Krämer, S. D.; Schibli, R.; Marottoli, R.; Perrone, R.; Berardi, F.; Niso, M.; Ametamey, S. M. Development of 3,4-dihydroisoquinolin-1(2H)-one derivatives for the Positron Emission Tomography (PET) imaging of σ_2 receptors. *Eur. J. Med. Chem.* **2013**, *69*, 920–930.

46. Berardi, F.; Ferorelli, S.; Abate, C.; Colabufo, N. A.; Contino, M.; Perrone, R.; Tortorella, V. 4-(Tetralin-1-yl)- and 4-(Naphthalen-1-yl)alkyl Derivatives of 1-Cyclohexylpiperazine as σ Receptor Ligands with Agonist σ2 Activity. *J. Med. Chem.* **2004**, *47*, 2308–2317.

47. Fanizza, E.; Urso, C.; Pinto, V.; Cardone, A.; Ragni, R.; Depalo, N.; Curri, M. L.; Agostiano, A.; Farinola, G. M.; Striccoli, M. Single white light emitting hybrid

nanoarchitectures based on functionalized quantum dots. *J. Mater. Chem. C* **2014**, *2*, 5286–5291.

48. Fanizza, E.; Altomare, M.; Di Mauro, A. E.; Del Sole, T.; Corricelli, M.; Depalo, N.; Comparelli, R.; Agostiano, A.; Striccoli, M.; Curri, M. L. Polyelectrolyte Multilayers As a Platform for Luminescent Nanocrystal Patterned Assemblies. *Langmuir* **2012**, *28*, 5964–5974.
49. Abate, C.; Niso, M.; Marottoli, R.; Riganti, C.; Ghigo, D.; Ferorelli, S.; Ossato, G.; Perrone, R.; Lacivita, E.; Lamb, D. C.; Berardi, F. Novel Derivatives of 1-Cyclohexyl-4-[3-(5-methoxy-1,2,3,4-tetrahydronaphthalen-1-yl)propyl]piperazine (PB28) with Improved Fluorescent and σ Receptors Binding Properties. *J. Med. Chem*. **2014**, *57*, 3314–3323.
50. Niso, M.; Riganti, C.; Pati, M. L.; Ghigo, D.; Berardi, F.; Abate, C. Novel and Selective Fluorescent σ2-Receptor Ligand with a 3,4-Dihydroisoquinolin-1-one Scaffold: A Tool to Study σ2 Receptors in Living Cells. *Chembiochem.* **2015**, *16*, 1078–1083.
51. Fisher, M. J.; Gunn, B.; Harms, C. S.; Kline, A. D.; Mullaney, J. T.; Nunes, A.; Scarborough, R. M.; Arfsten, A. E.; Skelton, M. A.; Um, S. L.; Utterback, B. G.; Jakubowski, J. A. Non-peptide RGD surrogates which mimic a Gly-Asp beta-turn: potent antagonists of platelet glycoprotein IIb-IIIa. *J. Med. Chem.* **1997**, *40*, 2085–2101.
52. Abate, C.; Ferorelli, S.; Niso, M.; Lovicario, C.; Infantino, V.; Convertini, P.; Perrone, R.; Berardi, F. 2-Aminopyridine Derivatives as Potential σ2 Receptor Antagonists. *Chem. Med. Chem.* **2012**, *7*, 1847–1857.
53. Zeng, C.; Vangveravong, S.; Xu, J.; Chang, K. C.; Hotchkiss, R. S.; Wheeler, K. T.; Shen, D.; Zhuang, Z. P.; Kung, H. F.; Mach, R. H. Subcellular localization of sigma-2

receptors in breast cancer cells using two-photon and confocal microscopy. *Cancer Res.* **2007**, *67*, 6708–6716.

54. Chakraborty, A.; Jana, N. R. Design and Synthesis of Triphenylphosphonium Functionalized Nanoparticle Probe for Mitochondria Targeting and Imaging. *J. Phys. Chem. C* **2015**, *119*, 2888–2895.
55. Fröhlich, E. The role of surface charge in cellular uptake and cytotoxicity of medical nanoparticles. *Int. J. Nanomedicine* **2012**, *7*, 5577–5591.
56. Shahabi, S.; Treccani, L.; Dringen, R.; Rezwan, K. Modulation of Silica Nanoparticle Uptake into Human Osteoblast Cells by Variation of the Ratio of Amino and Sulfonate Surface Groups: Effects of Serum. *ACS Appl. Mater. Interfaces* **2015**, *7*, 13821–13833.

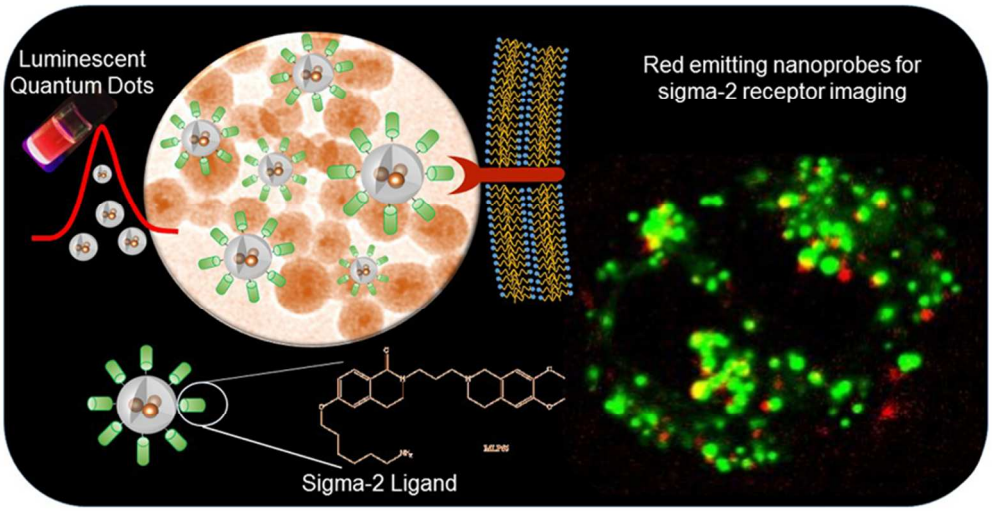

285x149mm (90 x 90 DPI)